Management of breather interactions

Andrey Gelash [ORCID],[*] Gang Xu [ORCID],[†] and Bertrand Kibler [ORCID]

Laboratoire Interdisciplinaire Carnot de Bourgogne (ICB),
UMR 6303 CNRS-Université Bourgogne Franche-Comté, 21078 Dijon, France

We propose theoretically and confirm experimentally a general approach to manage multiple nonlinear interactions of coherent solitary wave structures on an unstable background—breathers. It allows adjusting the initial positions and phases of more than two moving breathers to observe various desired wave states at controllable moments of wave evolution. Our theoretical framework relies on exact multibreather solutions to the one-dimensional focusing nonlinear Schrödinger equation and asymptotic expressions describing shifts of breather positions and phases acquired by them in mutual collisions. As proof-of-principle, we consider a couple of separated pairs of breathers initially synchronized in a small-amplitude patterns; meanwhile, our approach can be generalized to other breather types and wave states. We obtain an explicit expression for the separation interval between the pairs so that the interactions of the breathers from the neighboring patterns lead to the formation of an extreme amplitude wave or recurrence to the initial small-amplitude state. Experiments are carried out on a light wave platform with a nearly conservative optical fiber system, which accurately reproduces the predicted dynamics and proves the viability of our nonlinear wave theory.

I. INTRODUCTION

Coherent nonlinear solitary wave structures on an unstable background such as breathers, have received much attention in theoretical and experimental studies over the past several decades, see e.g., Refs. [1–3]. Breathers being a generalization of the soliton concept, exhibit an exciting picture of propagations and collisions, thanks to the instability features of the background [4–6]. The key nonlinear model to describe the breathers behavior in nonlinear media is the focusing one-dimensional nonlinear Schrödinger equation (NLSE), which in dimensionless form reads as

$$i\psi_\xi + \tfrac{1}{2}\psi_{\tau\tau} + |\psi|^2\psi = 0. \tag{1}$$

Here $\psi(\xi, \tau)$ describes complex-valued wave field, ξ and τ are the scaled propagation distance and time, respectively. The NLSE represents a universal model of nonlinear physics, which describes the propagation of weakly nonlinear waves in various media ranging from optical fibers and fluids to Bose-Einstein condensates [2,7,8]. As typically done, the unstable background is modeled by a simple solution of Eq. (1) $\psi_0 = Ae^{iA^2\xi}$, where A is the background amplitude, which we set to unity. The wave field ψ_0 is modulationally unstable to long-wave harmonic perturbations having wave vectors $k \in (-2, 2)$, see [9–11] for more information on the modulation instability (MI) phenomena. Note that we write the NLSE in the fashion of optical studies so that the propagation distance plays the role of the evolution variable.

The NLSE, completely integrable using inverse scattering transform (IST) technique [12], allows finding exact single and multiple breather solutions [13–18]. Among various solutions of Eq. (1), the most widely known are breathers of Akhmediev, Kuznetsov, Peregrine, and Tajiri-Watanabe [13–18]. While Akhmediev breathers represent periodic in τ solutions, the general breathers are oscillating coherent localized structures moving on the unstable background. Single breathers have been thoroughly studied and now have become classical models of nonlinear wave motion, in particular, the development of MI and formation of extreme amplitude (rogue) waves [1,13,17,19–22]. On the other hand, multibreathers exhibit more complex behavior, which includes formation of high-order rogue waves, molecule bound states and the so-called superregular scenario of the MI development [5,6,23–26]. In addition, the interest in propagation of spontaneously generated waves, brings to the agenda the problem of breathers with random parameters [27–30]. Most importantly, the nonlinear dynamics described by breather solutions can be observed in nature, which pioneering experimental studies [20,21,31–33] on single Peregrine and Kuznetsov breathers have been confirmed in nonlinear optics, hydrodynamics, and plasma physics. Later on, other types of breathers, including high-order breathers and their interactions, have been investigated in different experimental settings, thus unveiling the rich physics of these pulsating nonlinear waves [6,24,34–38].

Stable propagations and nontrivial interactions are two sides of one coin in nonlinear coherent structures. For example, governing by relative phase, the NLSE solitons exhibit

---

*Andrey.Gelash@u-bourgogne.fr

†Present address: School of Optical and Electronic information, Huazhong University of Science and Technology, Wuhan, Hubei 430074, China

a broad family of interaction profiles different from those emerging in linear wave fields interference. In particular, the so-called "in-phase" synchronization leads to a local nonlinear wave field compression with a peak power corresponding to the sum of the interacting solitons amplitudes. Meanwhile, the high-order (nonintegrable) corrections to the NLSE model, which always occur in real-life experiments, trigger such nonelastic effects as soliton fusions and annihilations, energy exchange, and supercontinuum generation [39–43]. In the matter of breathers, the ratio of the amplitudes between the collision profile and the background wave is the focus of studies. Collisions of breathers can produce both small-amplitude background perturbation and high amplitude wave field amplification, depending on the relative phase [5,23,36]. When these states follow each other, one can see it as a fascinating nonlinear effect—the sudden formation of extreme waves from a calm background.

One usually distinguishes and observes experimentally the following three typical breather collision profiles: superregular (SR, minimum amplitude), rogue wave (RW, maximum amplitude), and ghost (GH, intermediate amplitude) (see Refs. [6,26,34,36]). Here we put forward to the agenda the problem of the theoretical and experimental management of these wave states in multiple subsequent breather collisions. In principle, the exact N-breather solution of the NLSE, where N is the number of breathers, see, e.g., [26,44], solves this issue as soon as they describe all the possible interaction pictures. However, multibreather complexes with $N > 2$ produce too intricate nonlinear dynamics that challenge us to find a simpler description. Here we analyze the asymptotic states of breathers before and after the collisions. Similar to conventional solitons (see, e.g., [45]), moving localized breathers interact elastically in the sense that after the collision, the number of breathers and their characteristics are the same as before, except specific position and phase shifts [46,47]. The asymptotic expressions describing the breather shifts have been found recently in Ref. [46], and later also derived in Refs. [47] and [48]. They allow one to configure the properties of the multibreather wave field, which lies down the theoretical background for the present paper. In particular, we derive a new theoretical expression for temporal separation between breather pairs, corresponding to the scenario when at certain (controllable) points of the propagation, the wave field represents either SR, GH, or RW profile. For example, the configuration, which we denote as SR $\rightarrow$ RW represents initial (for example, at $\xi = 0$) SR state of four breathers (two SR pairs separated by the time interval τ_{sh}, where sh stands for "synchronized"), which leads to the formation of synchronized collision in the RW phase at certain distance $\xi = \xi_{\text{sh}}$. Our theory provides exact expressions for the synchronized separation time and propagation distance τ_{sh} and ξ_{sh}. Based on the developed approach, we perform experiments in a nearly conservative optical fiber system for the configurations SR $\rightarrow$ RW and SR $\rightarrow$ SR, which accurately reproduces the obtained theoretical predictions. The presented examples show how multibreather complexes can be adjusted to form desired wave states at different moments of their evolution, introducing the concept of breather interactions management.

This paper is laid out as follows: in Sec. II, we show a general multibreather solution to the NLSE (1), explaining the meaning of all the solution parameters, and end up with a brief analysis of a single breather behavior. Then, in Sec. III we describe the collision of two NLSE breathers, demonstrate the emerging SR, GH, and RW profiles and provide the space-phase shifts formulas. In Sec. IV we present the theoretical background of the breather management, i.e., we configure phases and positions of the breathers to observe the desired states, such as SR, GH, or RW, at certain controllable moments of the wave field evolution. Finally, in Sec. V, we report the realization of the predicted breather collision dynamics in optical fiber experiments proving the viability of our theory. We summarize and discuss the results of the paper in Sec. VI. Additionally, in the Appendix we present details on the space-phase shifts formulas derivations, allowing one to reproduce the full theoretical scheme of the breather interaction management.

II. BREATHER SOLUTIONS OF THE NLSE

In this section we outline the basic theoretical information on the NLSE model of breathers. Each breather is characterized by four real valued parameters R, α, τ_0, θ and the background amplitude, which we set to unity, $A = 1$. As such, the general N-breather solution ψ^{NB} has $4N$ real valued parameters $\{R_1, \alpha_1, \tau_{0,1}, \theta_1; ...; R_N, \alpha_N, \tau_{0,N}, \theta_N\}$, where the subscripts distinguish each of the N breathers. It fully describes propagations and interactions of the breathers and can be represented in the following closed form (see, e.g., [5]):

$$\psi^{\text{NB}}(R_1, \alpha_1, \tau_{0,1}, \theta_1; ...; R_N, \alpha_N, \tau_{0,N}, \theta_N)$$

$$= e^{i\xi} \left\{ 1 + 2\det \begin{pmatrix} 0 & q_{1,2} & \cdots & q_{N,2} \\ q_{1,1}^* & & & \\ \vdots & & \widehat{M}^T & \\ q_{N,1}^* & & & \end{pmatrix} (\det\widehat{M})^{-1} \right\},$$

$$\tag{2}$$

where the matrix $\widehat{M}$ has the following elements:

$$\widehat{M}_{nm} = \frac{(\mathbf{q}_n \cdot \mathbf{q}_m^*)}{2\left(R_n e^{i\alpha_n} + \frac{e^{-i\alpha_n}}{R_n} - R_m e^{-i\alpha_m} - \frac{e^{i\alpha_m}}{R_m}\right)}. \tag{3}$$

In expressions (2) and (3) the subscripts $n = 1, .., N$, $m = 1, .., N$; while det stands for matrix determinant, index T means matrix transpose and the vectors $\mathbf{q}_n = (q_{n,1}, q_{n,2})$ have the following components:

$$q_{n1} = e^{-\phi_n^{\text{NB}}} - \frac{e^{\phi_n^{\text{NB}} - i\alpha_n}}{R_n}, \quad q_{n2} = e^{\phi_n^{\text{NB}}} - \frac{e^{-\phi_n^{\text{NB}} - i\alpha_n}}{R_n}, \tag{4}$$

with the phase function

$$\phi_n^{\text{NB}} = \eta_n(\tau - \tau_{0,n}) + \gamma_n \xi + i\left(k_n \tau + \delta_n \xi - \frac{\theta_n}{2}\right). \tag{5}$$

In the latter expression the coefficients are

$$\eta_n = -\frac{1}{2}\left(R_n - \frac{1}{R_n}\right)\cos\alpha_n,$$

$$k_n = -\frac{1}{2}\left(R_n + \frac{1}{R_n}\right)\sin\alpha_n,$$

$$\gamma_n = -\frac{1}{4}\left(R_n^2 + \frac{1}{R_n^2}\right)\sin 2\alpha_n,$$

$$\delta_n = \frac{1}{4}\left(R_n^2 - \frac{1}{R_n^2}\right)\cos 2\alpha_n. \tag{6}$$

Without loss of generality, we consider $-\pi/2 < \alpha < \pi/2$ and $R \geqslant 1$, since other values of these parameters describe the same class of solutions. Each nth breather has characteristic size l_n, such that

$$l_n^{-1} = |2\eta_n| = \left(R_n - \frac{1}{R_n}\right)|\cos\alpha_n|, \tag{7}$$

group velocity $V_{\text{gr},n}$ and frequency W_n,

$$V_{\text{gr},n} = -\frac{\gamma_n}{\eta_n} = -\frac{\sin\alpha_n(R_n^4 + 1)}{R_n(R_n^2 - 1)}, \tag{8}$$

$$W_n = -2\delta_n = -\frac{1}{2}\left(R_n^2 - \frac{1}{R_n^2}\right)\cos 2\alpha_n. \tag{9}$$

To get a feeling of the behavior of breathes, we consider the simplest exact single-breather solution of the NLSE ψ_{1B}. We omit the subscripts everywhere in Eq. (2) and for $N = 1$ obtain

$$\psi^{1B}(R, \alpha, \tau_0, \theta, \theta_g)$$
$$= \left(1 + 2\left(R + \frac{1}{R}\right)\cos\alpha \frac{q_1^* q_2}{|q_1|^2 + |q_2|^2}\right)e^{i\xi}e^{-i\theta_g}. \tag{10}$$

Note that, we added a general phase θ_g to the solution (10) multiplying it by $e^{-i\theta_g}$ [Eq. (1) is invariant to it], which is useful for further analysis. For the further derivations, we define the function (5) without subscripts as

$$\phi(R, \alpha, \tau_0, \theta) = \eta(\tau - \tau_0) + \gamma\xi + i\left(k\tau + \delta\xi - \frac{\theta}{2}\right). \tag{11}$$

The main parameters of the breather that are R and α control its shape, group velocity and frequency, see Eqs. (8) and (9). The other two parameters τ_0 and θ describe breather temporal position and phase, respectively. Note that θ cannot be written as a common multiplier (similar to θ_g) of the breather solution, being its internal phase, which affects the temporal profile $|\psi^{1B}(\tau)|$, see Eq. (10).

In general case when $R > 1$ and $\alpha \neq 0$, solution (10) describes temporally localized nonlinear coherent structure propagating on constant background—see Fig. 1 where its spatial-temporal plot and temporal profile at $\xi = 0$ are presented. The breather changes the background phase, so that the wave field has the following temporal asymptotics:

$$\psi^{1B}(\xi, \tau) \to -e^{i(\mp 2\alpha - \theta_g)} \quad \text{at} \quad \tau \to \pm\infty, \tag{12}$$

as shown in Fig. 1. The group velocity of the breather is proportional to $\sin\alpha$ following Eq. (8). At $\alpha = 0$ it becomes a standing oscillating object—the Kuznetsov breather
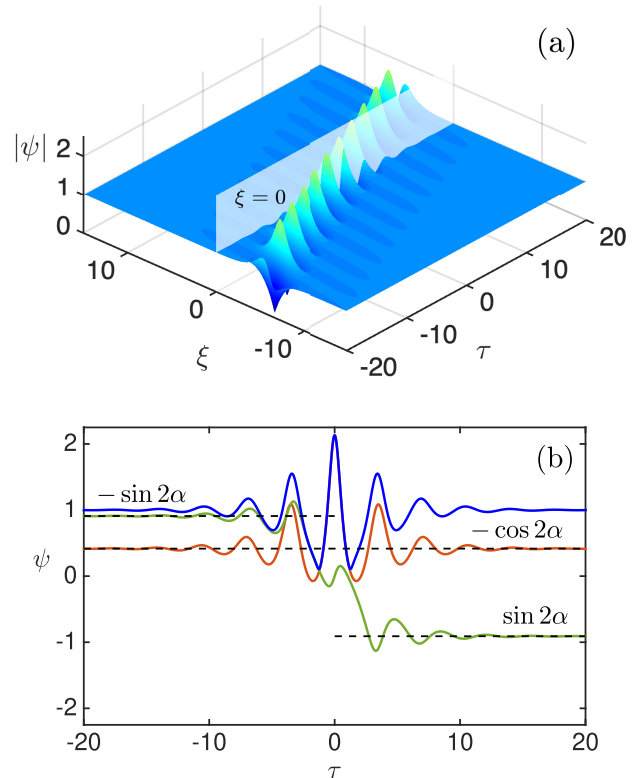

FIG. 1. General one-breather solution obtained from Eq. (10) at $R = 1.35$, $\alpha = -1.0$, $\theta = \pi$, $\tau_0 = 0$, and $\theta_g = 0$. (a) Spatial-temporal evolution of $|\psi|$. (b) Temporal profile at $\xi = 0$ corresponding to the cross section shown in (a): $|\psi|$ (blue line), Re[ψ] (real part of the wave field, red line), Im[ψ] (imaginary part of the wave field, green line). Horizontal black-dashed lines and expressions on the left and right sides of the plot (b) demonstrate asymptotic values of the wave filed according to Eq. (12).

[14–16]. For $R = 1$, solution (8) represents temporally periodic Akhmediev breather [13,23,49], which we do not consider in our paper since we focus on temporally localized objects.

III. INTERACTIONS OF TWO BREATHERS

Here we describe the interactions of two breathers, i.e., the solution (2) with $N = 2$. For moving breathers, the interaction process represents their collision followed by a temporal separation. Similar to solitons on zero background, the breathers interact elastically. After the collision, they restore their shape asymptotically (at large separation times) but acquire specific space and phase shifts. In contrast to soliton theory, where the shifts formulas were obtained together with the construction of the IST integration schemes [12,50], the breather shifts had been missed for a long time and were found recently in [46] and then in [47].

In this paper we focus on the pairs of temporally localized breathers with

$$R_1 = R_2 = R > 1; \quad \alpha_1 = -\alpha_2 = \alpha > 0, \tag{13}$$

that corresponds to the two-breather solution $\psi^{2B}(R, \alpha, \tau_{0,1}, \theta_1; R, -\alpha, \tau_{0,2}, \theta_2)$. Let us call the breathers

as first and second, following their subscripts 1 and 2. The solution in general has no symmetry in τ since the phase and position parameters are arbitrary. However the breathers have the same R and modulus of α, i.e., their main characteristics are similar. In particular the group velocity and breather frequency [see Eqs. (8) and (9)] can be written as

$$V_{\text{gr}} = V_{\text{gr},1} = -V_{\text{gr},2} < 0, \quad W = W_1 = W_2. \quad (14)$$

For the coefficients (6) we can also use the following simplified notations:

$$\eta = \eta_1 = \eta_2, \quad k = k_1 = -k_2,$$
$$\gamma = \gamma_1 = -\gamma_2, \quad \delta = \delta_1 = \delta_2, \quad (15)$$

so that the solution phases for the first and second breather [see Eq. (5)] can be written as

$$\phi_1^{2B} = \eta(\tau - \tau_{0,1}) + \gamma\xi + i(k\tau + \delta\xi - \theta_1/2),$$
$$\phi_2^{2B} = \eta(\tau - \tau_{0,2}) - \gamma\xi + i(-k\tau + \delta\xi - \theta_2/2). \quad (16)$$

The two breathers with parameters (13) move towards each other, then collide and separate. At large propagation distances $\xi \to \pm\infty$ before and after the collision, the solution represents a single breathers ψ_1^{1B} and ψ_2^{1B} (in this case, we apply the subscripts 1 and 2 to the solution ψ^{1B}, as before, to distinguish the first and second breather) with shifted τ_0 and θ parameters and shifted general phase,

$$\psi^{2B}(R, \alpha, \tau_{0,1}, \theta_1; R, -\alpha, \tau_{0,2}, \theta_2)$$

$$\to \begin{cases} \psi_1^{1B}, & \text{at} \quad \tau \sim V_{\text{gr}}\xi, \\ \psi_2^{1B}, & \text{at} \quad \tau \sim -V_{\text{gr}}\xi, \end{cases}$$

$$\psi_1^{1B} = \psi^{1B}(R, \alpha, \tau_{0,1} \mp \Delta\tau_0, \theta_1 \mp \Delta\theta, \mp\Delta\theta_{\text{g}}),$$
$$\psi_2^{1B} = \psi^{1B}(R, -\alpha, \tau_{0,2} \pm \Delta\tau_0, \theta_2 \pm \Delta\theta, \mp\Delta\theta_{\text{g}}). \quad (17)$$

Here the shifts $\Delta\tau_0$, $\Delta\theta$, $\Delta\theta_{\text{g}}$ can be obtained by simplification of the general formulas from [46] under the conditions (13) as

$$\Delta\tau_0 = \frac{R \ln\left[\frac{(R^2-1)^2}{\sin^2\alpha(R^4+2R^2\cos 2\alpha+1)}\right]}{2(R^2-1)\cos\alpha}, \quad (18)$$

$$\Delta\theta = \text{Arg}\left[\frac{2iR(R^2-1)\tan\alpha}{(1+R^2)^2\cos\alpha + i(R^4-1)\sin\alpha}\right], \quad (19)$$

$$\Delta\theta_{\text{g}} = (2\alpha + \pi), \quad (20)$$

see Appendix for the details. The asymptotic approximation (17) implies that the phases of the single-breathers (from the right hand side of the approximation expression) at $\xi \to \pm\infty$ can be written as

$$\phi_1^{1B} = \phi(R, \alpha, \tau_{0,1} \mp \Delta\tau_0, \theta_1 \mp \Delta\theta),$$
$$\phi_2^{1B} = \phi(R, -\alpha, \tau_{0,2} \pm \Delta\tau_0, \theta_2 \pm \Delta\theta). \quad (21)$$

Note that in expressions (21) and below, we also use the subscripts 1 and 2 for the single breather phases to distinguish them. To illustrate how the formulas (17)–(20) work, we approximate graphically the wave field profile of the second breather from ψ^{2B} at large propagation distances using the one-breather solution $\psi_2^{1B} = \psi^{1B}(R, -\alpha, \tau_0 + \Delta\tau_0, \theta + \Delta\theta, \theta_{\text{g}} + \Delta\theta_{\text{g}})$. In Fig. 2 one can see that the one-breather solution accurately reproduce both the wave field absolute
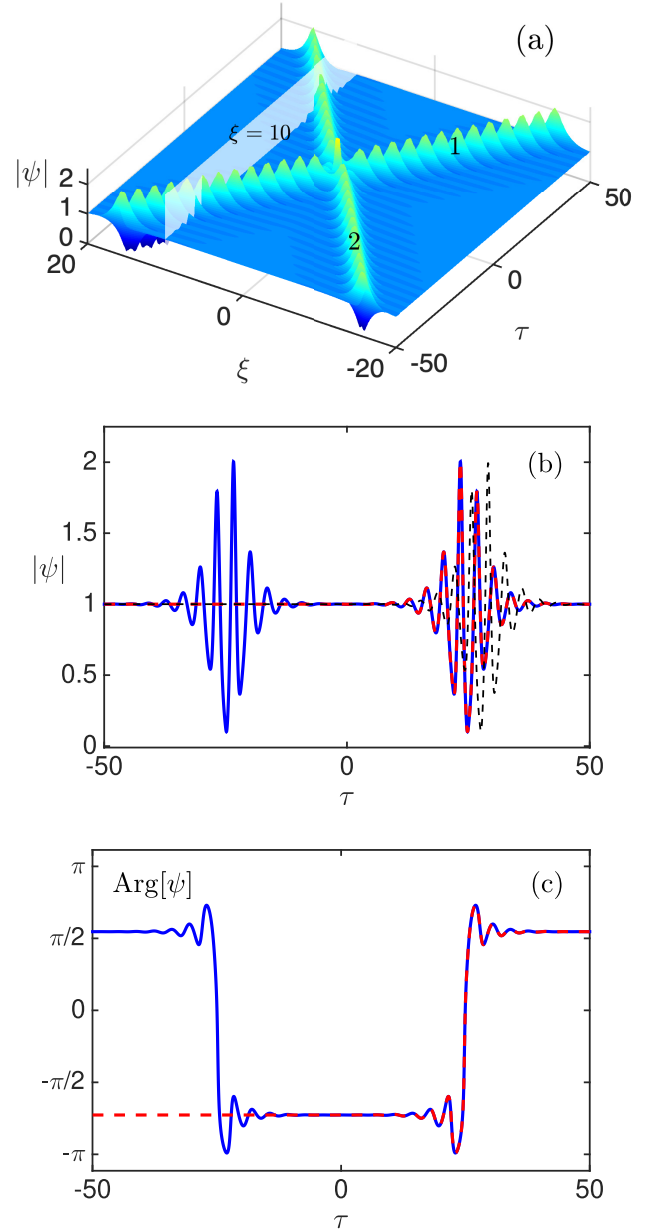

FIG. 2. Two-breather solution and its asymptotic state. (a) Spatial-temporal evolution of $|\psi|$. The numbers 1 and 2 denote the first and second breather. [(b), (c)] Temporal profiles of $|\psi|$ and the wave field phase argument $\text{Arg}[\psi]$ for the cross section at $\xi = 10$ shown in (a). Red dashed lines in (b) and (c) show the single-breather solution (10) approximating the asymptotic state of the second breather using formulas (17)–(20). Thin black-dashed line in (b) shows how the second breather would have looked like if it had been traveling alone. Breather parameters correspond to Eq. (13) with $R = 1.35$, $\alpha = 1.0$, and $\tau_{0,1} = \tau_{0,2} = 0$, $\theta_1 = \theta_2 = 0.025$.

value $|\psi^{2B}(\tau)|$ and its phase argument $\text{Arg}[\psi^{2B}(\tau)]$ in the vicinity of the second breather. In the next section, we will use similar approximations to manage multibreather interactions. In addition, Fig. 2(b) shows how the second breather would have looked like if it had been traveling alone, i.e., $\Delta\tau_0 = 0$, $\Delta\theta = 0$. Our comparison confirms both effects—the shifts of
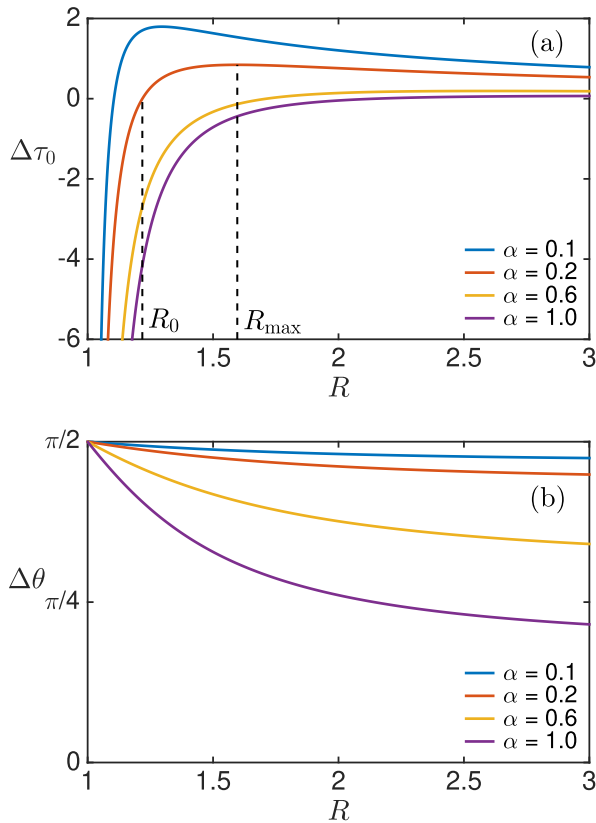
FIG. 3. Dependence of space (a) and phase (b) shifts $\Delta\tau_0$ and $\Delta\theta$ on the parameters R and α according to Eqs. (18) and (19). Vertical black-dashed lines in (a) show the points R_0 and $R_{\max}$, where the curve for $\alpha = 0.2$ reaches zero and maximum values correspondingly.

the breather temporal position and the phase. The latter effect leads to the change of the profile $|\psi^{2B}(\tau)|$.

Now let us briefly analyze the shifts formulas. According to Eqs. (18) and (19), $\Delta\tau_0$ and $\Delta\theta$ depend only on R and α. Figure 3 shows the functions $\Delta\tau_0(R)$ and $\Delta\theta(R)$ for a set of α values. In contrast to soliton theory, where the temporal shift is strictly positive, here it can be positive, negative, and even precisely zero, which means that breather can move forward or backward relative to its initial trajectory or remain on it see Fig. 3(a). To illustrate this issue in more detail, we design three representative collision scenarios characterized by positive, zero and negative temporal shifts and $\alpha = 0.2$, see Fig. 4. For the positive shift case we find numerically the point $R_{\max} = 1.596$ corresponding to the maximum of the function $\Delta\tau_0(R)$ (i.e., to the most pronounced temporal shift), while for the zero-shift case we find numerically $R_0 = 1.218$, such that $\Delta\tau_0(R_0) = 0$, see Figs. 4(a) and 4(b). The negative value of the temporal shift is unbounded at $R \to 1$, i.e., when the characteristic size l of the breather goes to infinity, see Eq. (7). In this case we choose $R = 1.1 < R_0$, that corresponds to a reasonable characteristic size l of the breathers, see Fig. 4(c).

Now we describe the family of the wave field profiles, which appear at the moment of breather collision and show how to manipulate them with the solution parameters. First let us note, that the two-breather wave field value taken at a point (ξ, τ), can be viewed as a single-valued function on its phases
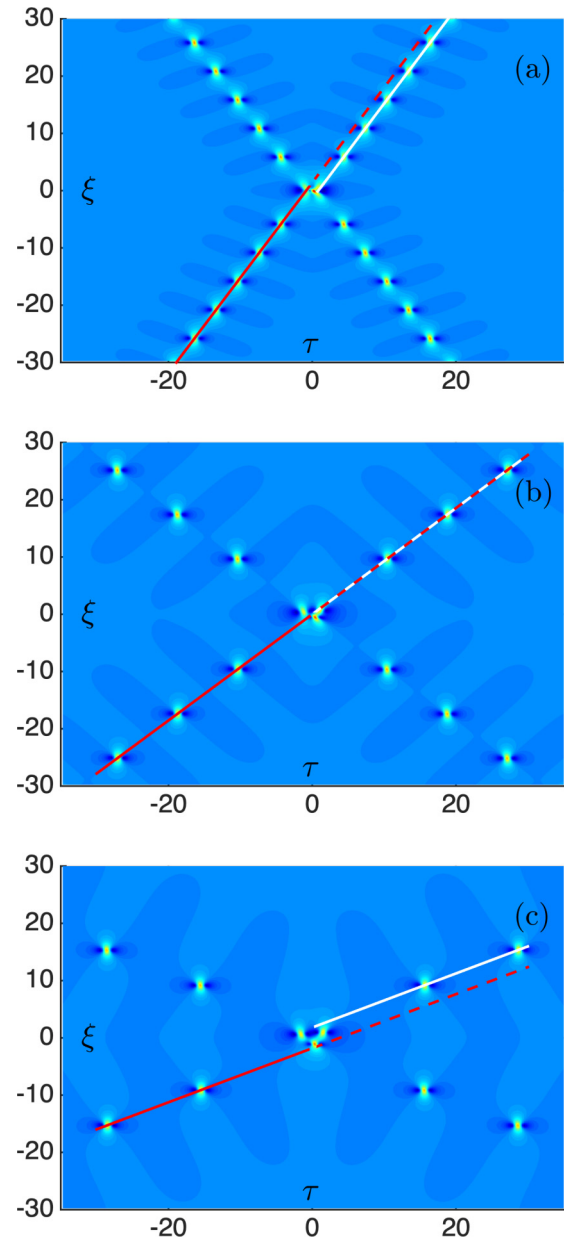

FIG. 4. Spatial-temporal evolution of $|\psi|$ for colliding breathers with (a) positive, (b) zero, and (c) negative temporal shifts $\Delta\tau_0(R)$. In all three cases $\alpha = 0.2$, while in (a) $R = R_{\max} = 1.596$, in (b) $R = R_0 = 1.218$, and in (c) $R = 1.1$. Straight-solid lines show trajectories of the second breather (red lines are used before the collision and white lines after) and red dashed-straight lines show which trajectory the breather would have been if the it had been traveling alone.

(5), i.e., $\psi^{2B} = \psi^{2B}(\phi_1^{2B}, \phi_2^{2B})$ with the following symmetry:

$$\psi^{2B}(\phi_1^{2B}, \phi_2^{2B}) = \psi^{2B}(\phi_2^{2B}, \phi_1^{2B}). \tag{22}$$

On the other hand, the linear algebraic system

$$\phi_1^{2B}(\xi, \tau) = a_1,$$
$$\phi_2^{2B}(\xi, \tau) = a_2, \tag{23}$$

where a_1 and a_2 are complex constants, is always nondegenerate with respect to variables ξ and τ since the corresponding
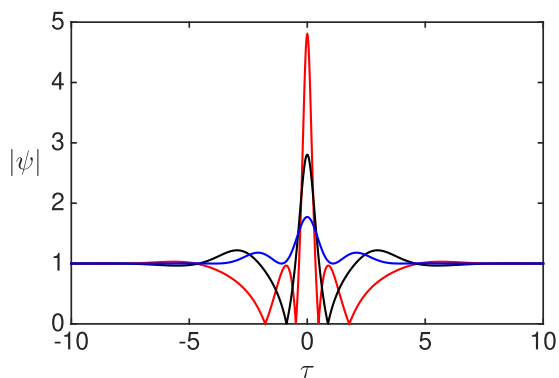
FIG. 5. Amplitude profiles at $\xi = 0$ for the basic cases of two-breather collision: superregular (SR, blue line), rogue wave (RW, red line), and ghost (GH, black line) phase synchronizations. The main breather parameters $R = 1.5$ and $\alpha = 0.5$, see Eq. (13); the collision point is $(\xi_c, \tau_c) = (0, 0)$ and the phases θ for each synchronization case are defined by (28).

determinant $\det = 2\eta(-\gamma + i\delta) \neq 0$. This means that in general, the same value of the wave field can be reached in two different points on the (ξ, τ) plane. At the same time by setting $a_1 = a_2$ we determine a distinctive point of the solution, i.e., a point with unique value of the wave field (like absolute maximum), since the symmetry (22) degenerates.

In our formalism the key role plays the distinctive point of the two-breather solution collision, which is defined as coordinates (ξ_c, τ_c), where the both phase functions have the value $-i\theta/2$,

$$\phi_1^{2B}(\xi_c, \tau_c) = \phi_2^{2B}(\xi_c, \tau_c) = -i\theta/2. \quad (24)$$

One can check that when the position-phase parameters obey the conditions

$$\tau_{0,1} = \tau_{0,2} = 0, \quad \theta_1 = \theta_2 = \theta, \quad (25)$$

the solution is temporally symmetric, i.e., $\psi^{2B}(\xi, \tau) = \psi^{2B}(\xi, -\tau)$, and its collision point is

$$(\xi_c, \tau_c) = (0, 0), \quad (26)$$

as expected for a solution with a symmetric choice of parameters and zero-temporal shifts.

In this case the phase θ represents a single degree of freedom for the two-breather solution with fixed parameters R and α. In particular, θ fully controls the collision profile $\psi_\theta^{2B}(0, \tau)$ at $\xi_c = 0$. At the center the profile reaches its maximum amplitude, which we call as collision amplitude a_c,

$$a_c = |\psi^{2B}(\xi_c, \tau_c)|. \quad (27)$$

We distinguish superregular (SR), ghost (GH), and rogue wave (RW) collision patterns (see e.g., [36]) that corresponds to the following choices of the phase:

$$\theta_{SR_{I,II}} = \{\pi/2; 3\pi/2\}, \quad \theta_{GH} = \pi, \quad \theta_{RW} = 0. \quad (28)$$

The SR and RW patterns exhibit minimum and maximum values for the collision amplitude a_c, and we also refer to them as annihilation and amplification scenarios, while the GH pattern correspond to an intermediate case, see Fig. 5. The SR pattern is also called "in-phase" synchronization. In

the GH case the wave field amplitude profile is close to those for a single breather with parameters R and α. The all three fundamental scenarios of the two-breather interactions have been studied in detail theoretically [5,23,38] and experimentally [36,38]. Note that $\psi_{SR_I}^{2B}(0, \tau)$ and $\psi_{SR_{II}}^{2B}(0, \tau)$ are complex conjugate to each other, what means that the evolution for SR_I is in reverse to those for SR_{II}.

We use the term rogue wave profile here in a general sense, namely as a wave of the maximum possible amplitude amplification for the chosen breathers. Meanwhile, a more specific term—rational rogue waves—corresponds to a class of exact solutions of the NLSE expressed in terms of a ratio of polynomial functions. Depending on the order j of the rational solution, its maximum amplitude can reach the values 3, 5, ... $2j + 1$, while the number of zeros of the wave field is 2, 4, ... $2j$, see [51]. The Peregrine solution is the first member of this family having $j = 1$. Rational RWs are benchmark solutions of the NLSE. As studied in [23,49,52,53], collisions of NLSE breathers or collisions of NLSE solitons lead to a local formation of close to rational ones wave field profiles with the number of zeros as in the rational case. In other words, for each rational rogue wave exists an infinite family of solutions exhibiting similar profiles at certain moments of evolution. The GH and RW profiles belong to the families of solutions close to the first and second-order rogue waves. Indeed, the number of zeros is 2 and 4, while the amplitude of the wave field maximum is near 3 and 5 correspondingly, see Fig. 5.

When $\varepsilon = R - 1 \lesssim 1$, the supperregular pattern represent a low-amplitude perturbation of the background, which can be approximated by the following formula (see [26]):

$$\psi(\tau) \approx 1 + 4i\varepsilon \frac{\cos\alpha \cos 2\eta\tau}{\cosh(2\varepsilon \cos\alpha)}. \quad (29)$$

From Eq. (29) we estimate the characteristic size of superregular pattern as

$$l_{SR} = (2\varepsilon \cos\alpha)^{-1}. \quad (30)$$

We do not have explicit estimations, similar to (30) for the characteristic sizes l_{RW} and l_{GH} corresponding to the RW and GH patterns. However, one can evaluate them by plotting the wave fields as in Fig. 5.

One can translate the two-breather solution in (ξ, τ) plane, moving its collision point from $(0,0)$ to nonzero coordinates (ξ_c, τ_c) by the following choice of the position-phase parameters:

$$\tau_{0,1} = \tau_c - V_{gr}\xi_c, \quad \tau_{0,2} = \tau_c + V_{gr}\xi_c,$$
$$\theta_1 = \theta + 2k\tau_c - W\xi_c, \quad \theta_2 = \theta - 2k\tau_c - W\xi_c. \quad (31)$$

We obtain these expressions by solving Eq. (23) with $a_1 = a_2 = -i\pi/2$ and $(\xi, \tau) = (\xi_c, \tau_c)$ with respect to $\tau_{0,1}$, $\tau_{0,2}$, θ_1 and θ_2. The parameters defined by Eqs. (13) and (31) correspond to a general two-breather solution symmetric in τ with respect to the point τ_c.

IV. MANAGEMENT OF BREATHER INTERACTIONS: THEORY

In this section, we present the theoretical concept of the management of more than two interacting moving breathers.

Our goal is to configure phases and positions of the breathers so that during evolution, the multibreather complex represents certain phase synchronization patterns, such as SR, RW, or GH. When dealing with $N > 2$, the mutual shifts acquired by the breathers change the simple phase synchronization conditions (28), so that an additional theoretical consideration is required.

As proof-of-principle we build a four-breather complex, exhibiting at the initial (sub- and superscripts i) and final (sub- and superscripts f) stages of its evolution the wave field patterns with θ_i and θ_f. More specifically we linearly add to each other two identical two-breather patterns with $\theta = \theta_i$ separated by $\tau_{sh} \gtrsim l_i$, where sh stands for "synchronized" and l_i is the characteristic size of the pattern. We take advantage of the significant initial separation between the patterns, which allows us to independently apply the breather shifts formulas to each breather pair. Note that in terms of the IST theory, the initial condition we build is close to a degenerate case when the main breather parameters coincide (but not precisely it since we have the patterns overlapping), see, e.g., [54,55]. The degenerate limit in the phase-shift formulas is an interesting mathematical question, which we leave for further studies.

The first pattern has the collision point $(0,0)$, while the second one corresponds to the collision point $(0, \tau_{sh})$. We chose τ_{sh} large enough to observe emerging of individual breathers from the initial conditions, so that at certain propagation distance ξ_{sh}, a couple of breathers from the neighboring patterns collide. Our goal is to find τ_{synch}, so that the colliding breathers generate the new patterns with $\theta = \theta_f$ at $\xi = \xi_{sh}$. According to the solution symmetry in τ, the breather 2 from the first pattern, and the breather 1 from the second pattern, produce two breathers moving symmetrically towards each other and then collide at $\tau = \tau_{sh}/2$.

When the breathers emerged from the initial patterns pronouncedly separate, one can describe the colliding ones by the two-breather solution with the phase θ_f and the collision point $(\xi_{sh}, \tau_{sh}/2)$. The idea of the breather interaction management is to choose $\delta\tau_{sh}$ so that the single breathers 2 and 1 from the first and second initial patterns are precisely the same as the breathers 2 and 1 from the desired final pattern, see our illustration of the synchronization process in Fig. 6. The same breathers means the same solution phases. According to Eq. (21) taken at $\xi \to +\infty$, the solution phase for the second breather from the first initial pattern is

$$
\begin{aligned}
\phi_2^{1B,i} &= \phi(R; -\alpha; \Delta\tau_0; \theta_i + \Delta\theta) \\
&= \eta(\tau - \Delta\tau_0) - \gamma\xi + i(-k\tau + \delta\xi - (\theta_i + \Delta\theta)/2).
\end{aligned}
\tag{32}
$$

Meanwhile, the solution phase for the second breather from the final pattern for the collision point $(\xi_{sh}, \tau_{sh}/2)$, see Eq. (21) at $\xi \to -\infty$ and Eq. (31), is

$$
\begin{aligned}
\phi_2^{1B,f} &= \phi(R; -\alpha; \tau_{sh}/2 + V_{gr}\xi_{sh} - \Delta\tau, \\
&\quad \times \ \theta_f - k\tau_{sh} - W\xi_{sh} - \Delta\theta) \\
&= \eta(\tau - \tau_{sh}/2 - V_{gr}\xi_{sh} + \Delta\tau) - \gamma\xi \\
&\quad + i(-k\tau + \delta\xi - (\theta_f - k\tau_{sh} - W\xi_{sh} - \Delta\theta)/2).
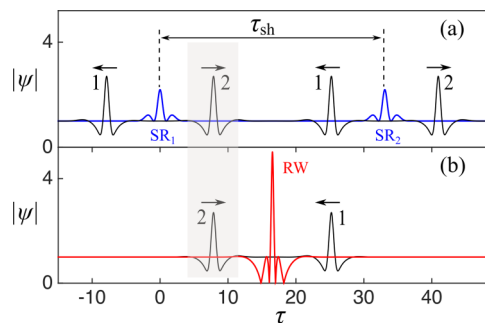\end{aligned}
\tag{33}
$$

FIG. 6. Illustration of the breather interaction management. The initial SR patterns (i = SR) located at $\xi = 0$ (SR$_1$) and τ_{sh} (SR$_2$), see panel (a), blue lines. The final (desired) state represents collision of the breathers producing the RW pattern (f = RW) at $\xi = \xi_{sh}$, see panel (b), red lines. The black lines in (a) and (b) show single breathers from the patterns at an intermediate (between the initial and final state) propagation distance, while horizontal arrows indicate the breather propagation direction. We choose $\delta\tau_{sh}$ according to Eq. (35), so that the single breathers 2 and 1 from the first and second initial patterns are precisely the same as the breathers 2 and 1 from the final pattern, what formally writes as equality (34). The vertical-gray band highlight this correspondence. Breather parameters correspond to Eq. (13) with $R = 1.7$, $\alpha = 0.5$; the initial separation computed using formula (35) for $\theta_i = \theta_{SR}$, $\theta_f = \theta_{RW}$ and $m = 3$.

According to our assumption, the second breather from the first initial pattern and the second breather from the final pattern are identical, so that

$$
\phi_2^{1B,i}(\xi, \tau) \equiv \phi_2^{1B,f}(\xi, \tau).
\tag{34}
$$

Finally, from equality (34) we obtain the following synchronization formulas:

$$
\xi_{sh} = \frac{\theta_f - \theta_i - 2\Delta\theta - 4k\Delta\tau_0 - 2\pi m}{W - 2kV_{gr}},
\tag{35}
$$

$$
\tau_{sh} = \frac{4W\Delta\tau_0 - 2V_{gr}(\theta_f - \theta_i - 2\Delta\theta - 2\pi m)}{W - 2kV_{gr}},
\tag{36}
$$

where m is an integer number, which we chose so that $\tau_{sh} \gtrsim l_i$ (the other choices are nonphysical). One can interpret the proposed approach as follows. The second breather from the first pattern, see Fig. 6, acquires a phase-position shift when interacting with its neighbor (breather 1 in the first pattern), which we compensate by adjusting the distance to the second pattern in such a way that the subsequent breather collision appears in the desired phase.

Using the above synchronization formulas, we can generate the initial multibreather states and predict the propagation distance where we observe the synchronized collision. To test our theory, we construct the initial conditions for i = SR and f = RW/SR with a negligible overlapping between the initial SR patterns. Then we run numerical simulations of the wave field evolution using the standard split-step Fourier method for the NLSE (1) with periodic boundary conditions related to τ_{sh}. The application of the periodic boundary conditions does not change the behavior of the colliding breathers at the center of the simulation interval since the initial patterns are identical and symmetric. Figure 7 shows the simulation results, which accurately verify our synchronization procedure. In the case,
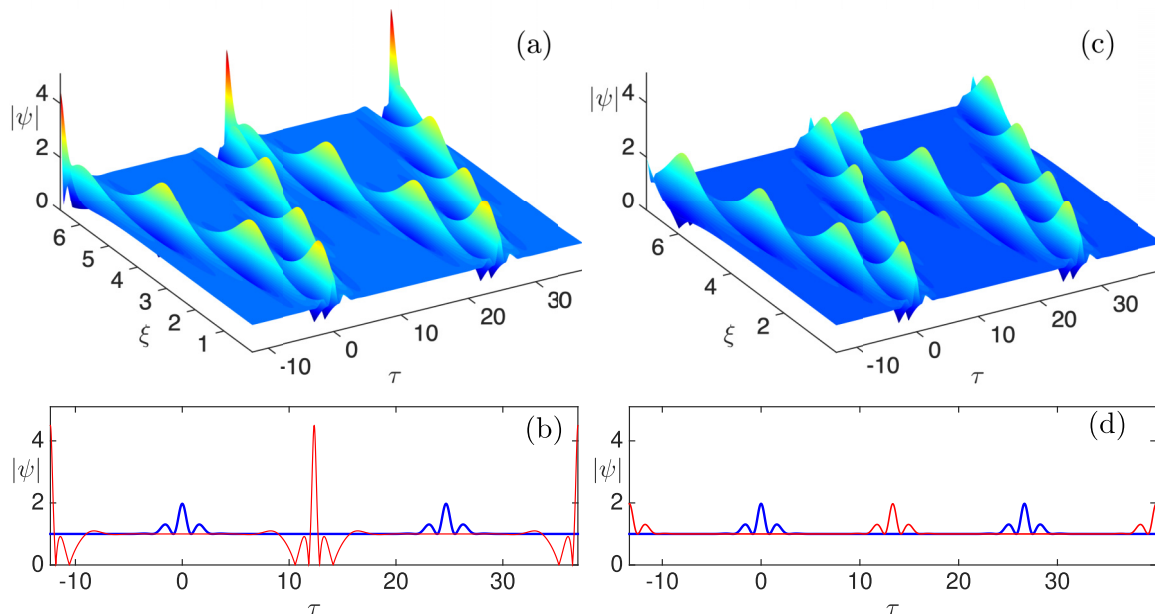
FIG. 7. Numerical simulations of the synchronized breather interactions. The initial SR_{II} patterns correspond to Eq. (13) with parameters $R = 1.7$ and $\alpha = 0.7$. The separation between them computed using formula (35) with $\theta_i = \theta_{SR_{II}}$, and [(a), (b)] $\theta_f = \theta_{RW}$, $m = 2$; [(c),(d)] $\theta_f = \theta_{SR}$, $m = 3$. Panels (a) and (c) show evolution diagram ranged from 0 to ξ_{sh}, while panels (b) and (d) show the corresponding initial ($\xi = 0$, blue line) and final ($\xi = \xi_{sh}$, red line) wave field patterns.

f = RW we observe the formation of the rogue wave profile [see Figs. 7(a) and 7(b)], while in the case f = SR we observe the recurrence to the initial SR state.

V. MANAGEMENT OF BREATHER INTERACTIONS: EXPERIMENT

This section reports the experimental realization of the breather interactions management concept. We perform experiments in a nearly conservative optical fiber system described by the NLSE model. Our experiment setup is depicted in Fig. 8, which is based on commercially available equipment of the telecommunication industry. A home-made frequency-comb source with 20-GHz line spacing centered near 1550 nm is launched into a silicon-based programmable filter (wave shaper), which performs accurate line-by-line spectral shaping, including intensity attenuation and phase
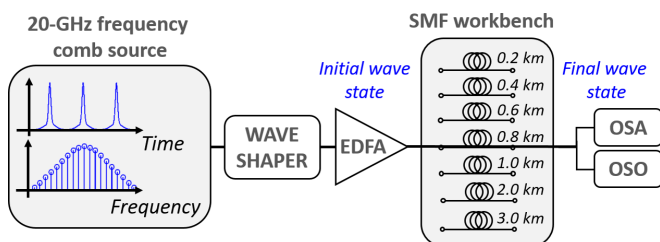

FIG. 8. Experimental setup based on a light wave platform with a nearly conservative optical fiber system. EDFA: erbium-doped fiber amplifier; SMF: single-mode fiber; OSA: optical spectrum analyzer; OSO: optical sampling oscilloscope

delay. The resulting periodic shaped pulse train is amplified by a high-power erbium-doped fiber amplifier to achieve the exact excitation of the multibreather solution of the NLSE in terms of average power for nonlinear propagation into a standard single-mode fiber (SMF). The nonlinear propagation is investigated throughout different lengths of the same fiber, and the output waveforms are characterized by means of a sub-ps-resolution optical sampling oscilloscope (OSO) in time domain and a high dynamic range optical spectrum analyzer (OSA) in spectral domain. Our standard fiber used for breather propagation exhibits the following features: an anomalous group-velocity dispersion $\beta_2 = -21 \, \text{ps}^2/\text{km}$, linear losses $\alpha = 0.2 \, \text{dB/km}$, and a nonlinear coefficient $\gamma = 1.1/\text{W/km}$. Fiber characteristics were chosen in accordance with both spectral bandwidth and peak power of the wave evolving into the fiber in order to avoid any detrimental higher-order dispersive or nonlinear effect. The correspondence between theory and experiment can be retrieved by recalling that the dimensional distance z (m) and time t (s) are related to the previous normalized parameters by $z = \xi L_{nl}$ and $t = \tau t_0$. Here the characteristic (nonlinear) length and the time scale are $L_{nl} = (\gamma P_0)^{-1} \sim 1335 \, \text{m}$ and $t_0 = \sqrt{|\beta_2| L_{nl}} \sim 5.16 \, \text{ps}$, respectively. The dimensional optical field $A(z, t)$ (in unit of $\text{W}^{\frac{1}{2}}$) is $A = \sqrt{P_0} \psi$, P_0 being the average power of the perturbed continuous wave, here is about 0.63 W.

For experimental verification of the breather management theory we consider the synchronized scenarios with i = SR, while f = RW/SR. We adjust parameters R, α, and m, such that both the temporal separation between the initial patterns τ_{sh} and the propagation distance ξ_{sh} fit our experimental setup, see Table I. For the found parameters the overlapping between the breather patterns is more pronounced than those

TABLE I. Parameters of experimentally studied breathers. The temporal separation between the initial patters τ_{sh}, the distance between the formations of the initial and final patterns ξ_{sh}, and the collision amplitude a_c are presented in three variants: theoretical ("theory"), obtained in numerical simulations of the NLSE ("simul. **1**"), and obtained in numerical simulations of the NLSE with losses ("simul. **2**"). The latter has been used for the optical signal generation.

–	i = SR, f = RW	i = SR, f = SR
R	1.57	2.0
α	0.65	0.65
m	0	1
τ_{sh}, theory	9.65	9.56
τ_{sh}, simul. **1/2**	9.60/9.67	9.56/9.69
ξ_{sh}, theory	2.85	2.67
ξ_{sh}, simul. **1/2**	2.80/2.92	2.67/2.72
a_c, theory	4.51	2.59
a_c, simul. **1/2**	4.38/3.91	2.53/2.61

considered in Fig. 7, leading, together with fiber losses, to corrections of the synchronization formulas (35) and (36).

To investigate the corrections, we perform optimization procedures through numerical simulations of the standard NLSE (1) and the following modified NLSE, which accounts for the fiber losses:

$$i\psi_\xi + \tfrac{1}{2}\psi_{\tau\tau} + |\psi|^2\psi = -i\kappa\psi/2, \qquad (37)$$

where the dimensionless loss parameter is $\kappa = \alpha L_{nl}$. First, we run numerical simulations of the NLSE (1) for a set of values of the temporal separations between the initial patterns (simulation **1**), which are close to the theoretical one. For the case i = SR, f = RW we find numerical values of τ_{sh} and ξ_{sh} as maximum amplification amplitude during the breathers collision process. Meanwhile, for the case i = SR, f = SR we find numerical values of τ_{sh} and ξ_{sh} as minimum of the maximum wave field annihilation amplitudes. In addition, for

both cases, we measure numerical values of the collision amplitudes a_c. Then we repeat equivalent simulations within the modified model with fiber losses (simulation **2**) [see Eq. (37)], and summarize the obtained results in Table I. We find, that numerical values of τ_{sh} and ξ_{sh} in both simulations **1** and **2** are always close to their theoretical counterparts. Meanwhile, the collision amplitude for the pattern f = RW in the simulation **2** decreases by $\sim 13\%$ due to the loss effect. We use the values obtained from the simulation **2** with included fiber losses to investigate experimental propagation.

Figure 9 shows the corresponding dynamical evolution of both the amplification and the annihilation scenarios resulting from the collision phenomenon of moving breathers (see false color maps). We are able to create experimentally a periodic train of localized perturbations that subsequently evolves into pairs of breathers propagating in opposite directions. Adjacent moving breathers of the periodic pattern then collide. One can also observe in more details some of the selected wave profiles along the propagation [see Figs. 9(a) and 9(d)] that reproduce the desired snapshots towards the final RW and SR states. Measured experimental wave profiles are in excellent agreement with numerical predictions. Note that our segmented approach of wave evolution measurement (see Fig. 8) does not allow to measure precisely the final pattern at ξ_{sh}, but in its small vicinity.

VI. CONCLUSIONS

In this paper, we have shown how to configure theoretically and observe experimentally synchronized interactions of the NLSE breathers. First, we developed a theoretical framework based on the exact multibreather solutions to the NLSE and asymptotic expressions describing shifts of breather positions and phases acquired by them in mutual collisions. Then, using the shift formulas, we computed breather phases and positions such that during evolution, the wave field represents desired wave states, such as a small amplitude background perturbation or an opposite—nonlinear wave of high amplitude. Finally, we performed experiments on light breathers in a
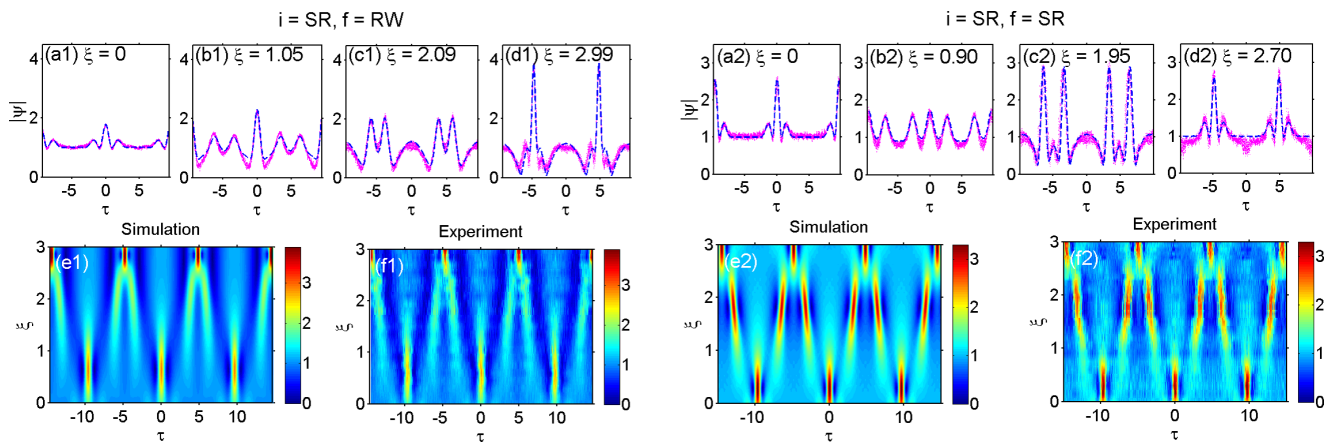

FIG. 9. Experimental measurements of the synchronized breather interactions. Left panels correspond to the case i = SR, f = RW; right panels to the case i = SR, f = SR. Snapshot in top rows [(a)–(d)] show wave field profiles at certain propagation distances. Numerical simulations of the NLSE with fiber losses are shown in blue dashed lines, while corresponding experimental measurements in tiny red dots. Color maps on the bottom rows [(e),(f)] show the space-time evolutions based on numerical simulations and experimental measurements. For the full set of the breather parameters see Table I.

nearly conservative optical fiber system, accurately reproducing the predicted wave field nonlinear dynamics.

Our approach is required when the number of managing breathers is more than two. Indeed, in the case $N = 2$, only one parameter—the relative phase, controls the pairwise breather interactions so that all the possible configurations, such as SR, RW, and GH, are well studied, see Sec. III. However, as soon as more breathers come into the game, the number of independent parameters increases by two additional parameters (phase and position with respect to the first pair) for each extra structure. Besides, when the interactions follow each other, the previous one changes the phase of the breather with which it enters the subsequent collision. In principle, a fitting of the multibreather solution parameters solves this issue. However, the increased number of parameters makes it unpractical and, at large N, even not possible. On the other hand, our approach provides an exact universal answer for the desired parameters of the multibreather complexes.

Regarding the IST theory, the breathers represent an important class of solutions of the NLSE, which corresponds to the discrete spectrum of the so-called auxiliary Zakharov-Shabat system [45,54]. The parameters of main breathers R and alpha are the coordinates of the discrete spectrum eigenvalue of the Zakharov-Shabat system, while the phase and position comprise the so-called norming constant. Together, the eigenvalues and norming constants form the scattering data—the nonlinear wave field's IST spectral portrait. Other classes of the scattering data are represented by degenerate eigenvalues, continuous spectrum (nonlinear dispersive waves) and finite bands (various quasi-periodic waves), which are also under active studies [2,55,56]. In this light, the management of breather interactions allows one to manipulate the properties of the nonlinear wave field by adjusting scattering data. Similar ideas have recently emerged in related areas of research of the IST studies; see the papers on the generation of soliton and breather gases with controllable scattering data (nonlinear spectral synthesis of soliton/breather gases) [30,57,58], nonlinear spectral engineering of rogue waves [59], and on-demand generation of dark-bright solitons trains [60].

In this paper, we focused on identical temporally symmetric pairs of breathers, which allowed us to take advantage of the temporal periodicity of the light source in the experiment and observe the full breather collision dynamics in the available time slot. One can straightforwardly generalize our approach to other cases, such as synchronized collisions of moving breathers with the standing breathers of Peregrine and Kuznetsov. Our preliminary estimations show that experimentally a large temporal domain is needed to observe such interactions; what can be provided by hydrodynamical experimental setups for gravitational waves, see e.g., [36]. One can also generalize the breather interaction management concept to other integrable systems with breather solutions, such as vector NLSE model, where the breathers represent even richer family of nonlinear configurations [61–64]. Finally, we note that using the conditions on breather solution phases, see Eq. (34), allows one, in principle, to synchronize interactions of an arbitrary number of breathers of any type. In this case, an easy-to-solve system of linear algebraic equations on the solution phases [see Eq. (34)] appears. Its

solution provides the desired parameters of the breathers. Note that synchronization of a large ensemble of breathers is an important issue in studies of spontaneous modulation instability development, where the role of coherent structures in the wave field features is on the agenda of recent theoretical and experimental studies [28,65–69]. Also, one can similarly synchronize interactions of conventional solitons as the latter represents a limiting case of breathers on zero background. In summary, we believe that the proposed strategy will contribute to the studies of complex nonlinear phenomena by the design of novel synchronized multibreather and multisoliton configurations that significantly extend the known examples of phase synchronized interactions of the coherent structures [46,70–73].

APPENDIX

This Appendix provides supplementary information on the derivation of the breather position and phase shifts formulas, which we extensively use in the main part of the paper, see Eqs. (17)–(20). They represent two particular cases of the general expressions obtained previously in [46]. Note, that in our paper we use breather parameters R and α, meanwhile Ref. [46] characterizes breathers using complex parameters λ and ζ, which are connected to R and α as

$$\lambda = \frac{iA}{2}\left(Re^{i\alpha} + \frac{e^{-i\alpha}}{R}\right), \tag{A1}$$

$$\zeta = \frac{iA}{2}\left(Re^{i\alpha} - \frac{e^{-i\alpha}}{R}\right) = \sqrt{\lambda^2 + A^2}. \tag{A2}$$

Note that λ and the combination of R and α represent two major ways to parametrize discrete eigenvalues of the Zakharov-Shabat system. One can consider only the upper half of the λ plane, i.e., Im$[\lambda] > 0$ (or, equivalently, $-\pi/2 < \alpha < \pi/2$ and $R \geqslant 1$, see Sec. II), since other values of λ correspond to the same class of solutions. As typically done, we make the function $\zeta = \sqrt{\lambda^2 + A^2}$ branch cut on the interval $[-iA, iA]$, which differs from the automatic choice $\{[-i\infty, -iA] \cup [iA, \infty i]\}$ implied in software packets such as *Wolfram Mathematica*. In our case the branch cut is agreed with the parametrization (A2), so that for all considering values of λ we have Im$[\zeta] > 0$.

To make the present paper fully self-sufficient, we briefly explain the general derivations in variables λ and ζ, since the work [46] reports only the final answer and misses the details. Then we explain how to obtain the Eqs. (17)–(20) in variables α and R as a particular case of the general answer.

We begin with writing the general two-breather solution in variables λ and ζ (see [46]),

$$\psi^{2B}(\lambda_1, \tau_{0,1}, \theta_1; \lambda_2, \tau_{0,2}, \theta_2)$$

$$= e^{i\xi}\left\{ A + 2\det\begin{pmatrix} 0 & q_{1,2} & q_{2,2} \\ q_{1,1}^* & & \\ q_{2,1}^* & & \widehat{M}^T \end{pmatrix}(\det\widehat{M})^{-1} \right\}, \quad (A3)$$

where the matrix $\widehat{M}$ has the following elements:

$$\widehat{M} = \begin{pmatrix} \frac{(\mathbf{q}_1 \cdot \mathbf{q}_1^*)}{\lambda_1 - \lambda_1^*} & \frac{(\mathbf{q}_1 \cdot \mathbf{q}_2^*)}{\lambda_1 - \lambda_2^*} \\ \frac{(\mathbf{q}_2 \cdot \mathbf{q}_1^*)}{\lambda_2 - \lambda_1^*} & \frac{(\mathbf{q}_2 \cdot \mathbf{q}_2^*)}{\lambda_2 - \lambda_2^*} \end{pmatrix}, \quad (A4)$$

and the vectors $\mathbf{q}_n = (q_{n,1}, q_{n,2})$, $n = 1, 2$, have the following components:

$$q_{n1} = e^{-\phi_n} + \frac{iA}{\lambda_n + \zeta_n}e^{\phi_n}, \quad (A5)$$

$$q_{n2} = \frac{iA}{\lambda_n + \zeta_n}e^{-\phi_n} + e^{\phi_n},$$

with the phases

$$\phi_n^{2B} = u_n + iv_n, \quad (A6)$$

where

$$u_n = \text{Im}[\zeta_n](\tau - V_{\text{gr},n}\xi - \tau_{0,n}), \quad (A7)$$

$$v_n = -\text{Re}[\zeta_n]\tau - \text{Re}[\lambda_n\zeta_n]\xi - \theta/2. \quad (A8)$$

The group velocity $V_{\text{gr},n}$ in variables λ and ζ is

$$V_{\text{gr},n} = -\frac{\text{Im}[\lambda_n\zeta_n]}{\text{Im}[\zeta_n]}. \quad (A9)$$

We compare the asymptotic states of the two-breather solution (A3) and the single-breather solution, which in the variables λ and ζ reads as (we omit the subscript indexes)

$$\psi^{1B}(\lambda, \tau_0, \theta, \theta_g)$$

$$= \left(A + 2i(\lambda - \lambda^*)\frac{q_1^* q_2}{|q_1|^2 + |q_2|^2} \right)e^{i\xi}e^{-i\theta_g}. \quad (A10)$$

One can find that the background phase the following limit at $\tau \to \pm\infty$,

$$A + 2i(\lambda - \lambda^*)\frac{q_1^* q_2}{|q_1|^2 + |q_2|^2}$$

$$\to \begin{cases} \frac{\zeta^* + \lambda^*}{\zeta + \lambda}, & \text{if sign}(\tau) < 0 \\ \frac{\zeta + \lambda}{\zeta^* + \lambda^*}, & \text{if sign}(\tau) > 0, \end{cases} \quad (A11)$$

which allows one to find the asymptotics of the breather (A10) as

$$\psi^{1B} \to e^{\mp 2i\text{Arg}[\zeta + \lambda] - i\theta_g}, \quad \text{at} \quad \tau \to \pm\infty. \quad (A12)$$

One can check that the latter expression coincides with Eq. (12) after the variables changes (A1) and (A2).

To find the shifts of τ_0 and θ it is sufficient to study the determinants in the solutions (A3) and (A10). The determinant of the single-breather can be written as

$$|q_1|^2 + |q_2|^2 = \left(1 + \frac{A^2}{|\lambda + \zeta|^2} \right)(e^{-2u} + e^{2u})$$

$$+ iA\left(\frac{1}{\lambda + \zeta} - \frac{1}{\lambda^* + \zeta^*} \right)(e^{-2iv} + e^{2iv}). \quad (A13)$$

The determinant of the two-breather solution $\det\widehat{M}$ we study asymptotically. We denote one of the two breathers from the solution (A3) as breather j and another one as l, so that $j = 1$ or 2, while $l = 2$ or 1. Then consider the temporal region of the breather j at large distances, i.e., such τ and ξ that

$$\tau \sim V_{\text{gr},j}\xi, \quad \xi \to \pm\infty. \quad (A14)$$

In this case the real part of the phase functions of the breather l has the following behavior:

$$u_l \to \pm\infty, \quad \text{when} \quad r_l\text{sign}(\xi) = \pm 1, \quad (A15)$$

where $r_l = \pm 1$ is

$$r_l = \text{sign}(V_{\text{gr},l} - V_{\text{gr},j}). \quad (A16)$$

Note, that the expression $r_l\text{sign}(\xi)$ in (A15) represent the sign of u_l, see Eq. (A7).

Now let us for definiteness consider the case $u_l \to \infty$. Then

$$e^{\phi_l} \to \infty, \quad e^{-\phi_l} \to 0, \quad (A17)$$

so that the asymptotic components of the vector $\mathbf{q}_l$ can be simplified as

$$q_{l1} \to \frac{iA}{\lambda_l + \zeta_l}e^{\phi_l}, \quad q_{l2} \to e^{\phi_l}. \quad (A18)$$

The latter allows us to write the following asymptotic combinations as

$$(\mathbf{q}_l \cdot \mathbf{q}_l^*) \to e^{2u_l}\left(1 + \frac{A^2}{|\lambda_l + \zeta_l|^2} \right), \quad (A19)$$

and

$$(\mathbf{q}_l \cdot \mathbf{q}_j^*)(\mathbf{q}_j \cdot \mathbf{q}_l^*) \to e^{2u_l}\left(\frac{A^2}{|\lambda_l + \zeta_l|^2}|q_{j1}|^2 + |q_{j2}|^2 \right.$$

$$\left. - \frac{iA}{\lambda_l^* + \zeta_l^*}q_{j1}q_{j2}^* + \frac{iA}{\lambda_l + \zeta_l}q_{j2}q_{j1}^* \right). \quad (A20)$$

Now we can write the asymptotic determinant of the two-breather solution as

$$\det\widehat{M} \to e^{2u_l}\left\{ \frac{(1 + \frac{A^2}{|\lambda_l + \zeta_l|^2})(\mathbf{q}_j \cdot \mathbf{q}_j^*)}{(\lambda_l - \lambda_l^*)(\lambda_j - \lambda_j^*)} + \frac{\frac{A^2}{|\lambda_l + \zeta_l|^2}|q_{j1}|^2 + |q_{j2}|^2 - \frac{iA}{\lambda_l^* + \zeta_l^*}q_{j1}q_{j2}^* + \frac{iA}{\lambda_l + \zeta_l}q_{j2}q_{j1}^*}{|\lambda_l - \lambda_j^*|^2} \right\}. \quad (A21)$$

In addition, similar to Eq. (A12) one can find asymptotics of the two-breather solution as

$$\psi^{2B} \rightarrow \exp\{\mp 2i(\text{Arg}[\zeta_1 + \lambda_1] + \text{Arg}[\zeta_2 + \lambda_2])\}$$

$$\text{at} \quad \tau \rightarrow \pm\infty. \tag{A22}$$

Now we look for such combinations in (A21), that can be transformed into $(e^{-2u} + e^{2u})$ and $(e^{-2iv} + e^{2iv})$ [see Eq. (A13)] by a change of phase and position parameters. The first combination in (A21) reads as

$$e^{-2u_j}\sqrt{\frac{s_a - s_c}{s_b - s_d}} + e^{2u_j}\sqrt{\frac{s_b - s_d}{s_a - s_c}}$$

$$= e^{-2u_j + \frac{1}{2}\ln\left(\frac{s_a - s_c}{s_b - s_d}\right)} + e^{2u_j - \frac{1}{2}\ln\left(\frac{s_b - s_d}{s_a - s_c}\right)}. \tag{A23}$$

The second combination is

$$e^{-2iv_j + i\text{Arg}[i(p_a + p_b)]} + e^{2iv_j - i\text{Arg}[i(p_a + p_b)]}. \tag{A24}$$

The coefficients in Eqs. (A23) and (A24) have the following form:

$$s_a = (A^4 + |\lambda_l + \zeta_l|^2 \cdot |\lambda_j + \zeta_j|^2) \cdot |\lambda_l - \lambda_j^*|^2$$
$$+ A^2(|\lambda_l + \zeta_l|^2 + |\lambda_j + \zeta_j|^2) \cdot |\lambda_l - \lambda_j|^2,$$

$$s_b = A^2(|\lambda_l + \zeta_l|^2 + |\lambda_j + \zeta_j|^2) \cdot |\lambda_l - \lambda_j^*|^2$$
$$+ (A^4 + |\lambda_l + \zeta_l|^2 \cdot |\lambda_j + \zeta_j|^2) \cdot |\lambda_l - \lambda_j|^2,$$

$$s_c = A^2(\lambda_l - \lambda_l^*)(\lambda_j - \lambda_j^*) \cdot [(\lambda_l + \zeta_l)(\lambda_j + \zeta_j)$$
$$+ (\lambda_l^* + \zeta_l^*)(\lambda_j^* + \zeta_j^*)],$$

$$s_d = -A^2(\lambda_l - \lambda_l^*)(\lambda_j - \lambda_j^*) \cdot [(\lambda_l + \zeta_l)(\lambda_j^* + \zeta_j^*)$$
$$+ (\lambda_l^* + \zeta_l^*)(\lambda_j + \zeta_j)],$$

$$p_a = \{A^2(\lambda_j + \zeta_j - \lambda_l^* - \zeta_l^*) - |\lambda_l + \zeta_l|^2(\lambda_j^* + \zeta_j^*)$$
$$+ |\lambda_j + \zeta_j|^2(\lambda_l + \zeta_l)\}/\{|\lambda_l - \lambda_j^*|^2\},$$

$$p_b = \frac{(A^2 + |\lambda_l + \zeta_l|^2)(\lambda_j + \zeta_j - \lambda_j^* - \zeta_j^*)}{(\lambda_l - \lambda_l^*)(\lambda_j - \lambda_j^*)}.$$

Finally, we compare the computed combinations (A23) and (A24) with the determinant of the one-breather solution

(A13) and find that the two-breather solution at large distances before and after the collision point, i.e. at $\xi \rightarrow \pm\infty$, as two single-breather solutions with shifted τ_0 and θ parameters as follows:

$$\psi^{2B}(\lambda_1, \tau_{0,1}, \theta_1; \lambda_2, \tau_{0,2}, \theta_2)$$

$$\rightarrow \begin{cases} \psi_1^{1B}, & \text{at} \quad \tau \sim V_{\text{gr},1}\xi, \\ \psi_2^{1B}, & \text{at} \quad \tau \sim V_{\text{gr},2}\xi, \end{cases}$$

$$\times \psi^{1B}(\lambda_1, \tau_{0,1} \pm \Delta\tau_{0,1}, \theta_1 \pm \Delta\theta_1, \theta_{\text{g},1} \pm \Delta\theta_{\text{g},1}),$$

$$\times \psi^{1B}(\lambda_2, \tau_{0,2} \pm \Delta\tau_{0,2}, \theta_2 \pm \Delta\theta_2, \theta_{\text{g},2} \pm \Delta\theta_{\text{g},2}). \tag{A25}$$

where the shifts values are

$$\Delta\tau_{0,j} = r_l \frac{\ln[(s_a - s_c)/(s_b - s_d)]}{4\text{Im}[\zeta_j]}, \tag{A26}$$

$$\Delta\theta_j = r_l \text{Arg}[i(p_a + p_b)], \tag{A27}$$

$$\Delta\theta_{\text{g},j} = -2r_l \text{Arg}[\lambda_l + \zeta_l]. \tag{A28}$$

Note, that we find the general phase shift $\Delta\theta_{\text{g},j}$ analyzing the asymptotics (A22) and using that a single breather change the background phase by $2\text{sign}(\tau)2i\text{Arg}[\zeta + \lambda]$ according to Eq. (A12). The Eqs. (A25)–(A28) repeat the results obtained in [46] and in addition cover all the possible configurations of the breathers velocities by the sign r_l (Ref. [46] implied that the colliding breathers have opposite velocities).

The particular case considered in the main part of the paper [see Eq. (13)] boils down to the following choice of $\lambda_{1,2}$:

$$\lambda_1 = \frac{iA}{2}\left(Re^{i\alpha} + \frac{e^{-i\alpha}}{R}\right),$$

$$\lambda_2 = -\lambda_1^* = \frac{iA}{2}\left(Re^{-i\alpha} + \frac{e^{i\alpha}}{R}\right), \tag{A29}$$

One substitutes (A29) into the general expressions (A25)–(A28) and after straightforward simplifications ends up with the formulas (18)–(20).

[1] C. Kharif, E. Pelinovsky, and A. Slunyaev, *Rogue Waves in the Ocean, Observation, Theories and Modeling*, Advances in Geophysical and Environmental Mechanics and Mathematics Series (Springer, Heidelberg, 2009)

[2] A. Osborne, *Nonlinear Ocean Waves* (Academic Press, New York, 2010).

[3] S. Wabnitz, *Nonlinear Guided Wave Optics; A Testbed for Extreme Waves* (IOP Publishing, Bristol, 2017).

[4] N. N. Akhmediev and A. Ankiewicz, *Solitons: Nonlinear Pulses and Beams* (Springer, New York, 1997).

[5] V. E. Zakharov and A. A. Gelash, Nonlinear Stage of Modulation Instability, Phys. Rev. Lett. **111**, 054101 (2013).

[6] G. Xu, A. Gelash, A. Chabchoub, V. Zakharov, and B. Kibler, Breather Wave Molecules, Phys. Rev. Lett. **122**, 084101 (2019).

[7] Y. S. Kivshar and G. Agrawal, *Optical Solitons: From Fibers to Photonic Crystals* (Academic Press, Amsterdam, 2003).

[8] A. I. Maimistov and A. M. Basharov, *Nonlinear Optical Waves*, Vol. 104 (Kluwer Academic Publishers, London, 1999).

[9] T. B. Benjamin and J. E. Feir, The disintegration of wave trains on deep water, J. Fluid Mech. **27**, 417 (1967).

[10] V. E. Zakharov, Stability of periodic waves of finite amplitude on the surface of a deep fluid, J. Appl. Mech. Tech. Phys. **9**, 190 (1972).

[11] V. E. Zakharov and L. Ostrovsky, Modulation instability: The beginning, Physica D **238**, 540 (2009).

[12] V. Zakharov and A. Shabat, Exact theory of two-dimensional self-focusing and one-dimensional self-modulation of

waves in nonlinear media, Sov. Phys. JETP **34**, 62 (1972).

[13] N. N. Akhmediev, V. M. Eleonskii, and N. E. Kulagin, Generation of periodic trains of picoseconld pulses in an optical fiber: Exact solutions, Sov. Phys. JETP **62**, 894 (1985).

[14] E. A. Kuznetsov, Solitons in a parametrically unstable plasma, Sov. Phys. Dokl. **22**, 507 (1977).

[15] T. Kawata and H. Inoue, Inverse scattering method for the nonlinear evolution equations under nonvanishing conditions, J. Phys. Soc. Jpn. **44**, 1722 (1978).

[16] Y.-C. Ma, The perturbed plane-wave solutions of the cubic Schrödinger equation, Stud. Appl. Math. **60**, 43 (1979).

[17] D. H. Peregrine, Water waves, nonlinear Schrödinger equations and their solutions, J. Aust. Math. Soc. Series B, Appl. Math **25**, 16 (1983).

[18] M. Tajiri and Y. Watanabe, Breather solutions to the focusing nonlinear Schrödinger equation, Phys. Rev. E **57**, 3510 (1998).

[19] N. Akhmediev, A. Ankiewicz, and M. Taki, Waves that appear from nowhere and disappear without a trace, Phys. Lett. A **373**, 675 (2009).

[20] B. Kibler, J. Fatome, C. Finot, G. Millot, F. Dias, G. Genty, N. Akhmediev, and J. M. Dudley, The peregrine soliton in nonlinear fibre optics, Nat. Phys. **6**, 790 (2010).

[21] B. Kibler, J. Fatome, C. Finot, G. Millot, G. Genty, B. Wetzel, N. Akhmediev, F. Dias, and J. M. Dudley, Observation of Kuznetsov-Ma soliton dynamics in optical fibre, Sci. Rep. **2**, 463 (2012).

[22] B. Kibler, A. Chabchoub, and H. Bailung, Editorial: Peregrine soliton and breathers in wave physics: Achievements and perspectives, Front. Phys. **9**, 795983 (2021).

[23] N. Akhmediev, J. M. Soto-Crespo, and A. Ankiewicz, Extreme waves that appear from nowhere: On the nature of rogue waves, Phys. Lett. A **373**, 2137 (2009).

[24] A. Chabchoub, N. Hoffmann, M. Onorato, and N. Akhmediev, Super Rogue Waves: Observation of a Higher-Order Breather in Water Waves, Phys. Rev. X **2**, 011015 (2012).

[25] D. J. Kedziora, A. Ankiewicz, and N. Akhmediev, Classifying the hierarchy of nonlinear-schrödinger-equation rogue-wave solutions, Phys. Rev. E **88**, 013207 (2013).

[26] A. Gelash and V. E. Zakharov, Superregular solitonic solutions: A novel scenario for the nonlinear stage of modulation instability, Nonlinearity **27**, R1 (2014).

[27] M. Närhi, B. Wetzel, C. Billet, S. Toenger, T. Sylvestre, J.-M. Merolla, R. Morandotti, F. Dias, G. Genty, and J. M. Dudley, Real-time measurements of spontaneous breathers and rogue wave events in optical fibre modulation instability, Nat. Commun. **7**, 13675 (2016).

[28] J. M. Soto-Crespo, N. Devine, and N. Akhmediev, Integrable Turbulence and Rogue Waves: Breathers or Solitons?, Phys. Rev. Lett. **116**, 103901 (2016).

[29] A. R. Osborne, Breather turbulence: Exact spectral and stochastic solutions of the nonlinear Schrödinger equation, Fluids **4**, 72 (2019).

[30] G. Roberti, G. El, A. Tovbis, F. Copie, P. Suret, and S. Randoux, Numerical spectral synthesis of breather gas for the focusing nonlinear Schrödinger equation, Phys. Rev. E **103**, 042205 (2021).

[31] A. Chabchoub, N. P. Hoffmann, and N. Akhmediev, Rogue Wave Observation in a Water Wave Tank, Phys. Rev. Lett. **106**, 204502 (2011).

[32] H. Bailung, S. K. Sharma, and Y. Nakamura, Observation of Peregrine Solitons in a Multicomponent Plasma with Negative Ions, Phys. Rev. Lett. **107**, 255005 (2011).

[33] A. Chabchoub, B. Kibler, J. M. Dudley, and N. Akhmediev, Hydrodynamics of periodic breathers, Philos. Trans. R. Soc. A **372**, 20140005 (2014).

[34] B. Frisquet, B. Kibler, and G. Millot, Collision of Akhmediev Breathers in Nonlinear Fiber Optics, Phys. Rev. X **3**, 041032 (2013).

[35] B. Frisquet, A. Chabchoub, J. Fatome, C. Finot, B. Kibler, and G. Millot, Two-stage linear-nonlinear shaping of an optical frequency comb as rogue nonlinear-Schrödinger-equation-solution generator, Phys. Rev. A **89**, 023821 (2014).

[36] B. Kibler, A. Chabchoub, A. Gelash, N. Akhmediev, and V. E. Zakharov, Superregular Breathers in Optics and Hydrodynamics: Omnipresent Modulation Instability beyond Simple Periodicity, Phys. Rev. X **5**, 041026 (2015).

[37] A. Chabchoub, N. P. Hoffmann, E. Tobisch, T. Waseda, and N. Akhmediev, Drifting breathers and Fermi–Pasta–Ulam paradox for water waves, Wave Motion **90**, 168 (2019).

[38] G. Xu, A. Gelash, A. Chabchoub, V. E. Zakharov, and B. Kibler, Ghost interaction of breathers, Front. Phys. **8**, 608894 (2020).

[39] M. Islam, C. Soccolich, and J. Gordon, Ultrafast digital soliton logic gates, Opt. Quantum Electron. **24**, S1215 (1992).

[40] G. I. Stegeman and M. Segev, Optical spatial solitons and their interactions: Universality and diversity, Science **286**, 1518 (1999).

[41] A. Antikainen, M. Erkintalo, J. M. Dudley, and G. Genty, On the phase-dependent manifestation of optical rogue waves, Nonlinearity **25**, R73 (2012).

[42] D. Kachulin, A. Dyachenko, and A. Gelash, Interactions of coherent structures on the surface of deep water, Fluids **4**, 83 (2019).

[43] J. M. Dudley, G. Genty, and S. Coen, Supercontinuum generation in photonic crystal fiber, Rev. Mod. Phys. **78**, 1135 (2006).

[44] N. Akhmediev, V. Korneev, and N. Mitskevich, N-modulation signals in a single-mode optical waveguide under nonlinear conditions, Sov. Phys. JETP **67**, 89 (1988).

[45] S. Novikov, S. V. Manakov, L. P. Pitaevskii, and V. E. Zakharov, *Theory of Solitons: The Inverse Scattering Method* (Springer Science & Business Media, New York, 1984).

[46] A. A. Gelash, Formation of rogue waves from a locally perturbed condensate, Phys. Rev. E **97**, 022208 (2018).

[47] S. Li and G. Biondini, Soliton interactions and degenerate soliton complexes for the focusing nonlinear Schrödinger equation with nonzero background, Euro. Phys. J. Plus **133**, 400 (2018).

[48] G. El and A. Tovbis, Spectral theory of soliton and breather gases for the focusing nonlinear Schrödinger equation, Phys. Rev. E **101**, 052207 (2020).

[49] N. Akhmediev, J. M. Soto-Crespo, and A. Ankiewicz, How to excite a rogue wave, Phys. Rev. A **80**, 043818 (2009).

[50] M. J. Ablowitz and H. Segur, *Solitons and the Inverse Scattering Transform* (SIAM, Philadelphia, 1981), Vol. 4.

[51] N. Akhmediev, A. Ankiewicz, and J. M. Soto-Crespo, Rogue waves and rational solutions of the nonlinear Schrödinger equation, Phys. Rev. E **80**, 026601 (2009).

[52] D. Agafontsev and A. A. Gelash, Rogue waves with rational profiles in unstable condensate and its solitonic model, Front. Phys. **9**, 610896 (2021).

[53] A. Chabchoub, A. Slunyaev, N. P. Hoffmann, F. Dias, B. Kibler, G. Genty, J. Dudley, and N. Akhmediev, The Peregrine breather on the zero-background limit as the two-soliton degenerate solution: An experimental study, Front. Phys. **9**, 633549 (2021).

[54] V. E. Zakharov and A. B. Shabat, Exact theory of two-dimensional self-focusing and one-dimensional self-modulation of waves in nonlinear media, Sov. Phys. JETP **34**, 62 (1972).

[55] D. J. Kedziora, A. Ankiewicz, and N. Akhmediev, Second-order nonlinear Schrödinger equation breather solutions in the degenerate and rogue wave limits, Phys. Rev. E **85**, 066601 (2012).

[56] G. Biondini and D. Mantzavinos, Universal Nature of the Nonlinear Stage of Modulational Instability, Phys. Rev. Lett. **116**, 043902 (2016).

[57] A. A. Gelash and D. S. Agafontsev, Strongly interacting soliton gas and formation of rogue waves, Phys. Rev. E **98**, 042210 (2018).

[58] P. Suret, A. Tikan, F. Bonnefoy, F. Copie, G. Ducrozet, A. A. Gelash, G. Prabhudesai, G. Michel, A. Cazaubiel, E. Falcon, G. El, and S. Randoux, Nonlinear Spectral Synthesis of Soliton Gas in Deep-Water Surface Gravity Waves, Phys. Rev. Lett. **125**, 264101 (2020).

[59] A. Tikan, F. Bonnefoy, G. Roberti, G. El, A. Tovbis, G. Ducrozet, A. Cazaubiel, G. Prabhudesai, G. Michel, F. Copie, E. Falcon, S. Randoux, and P. Suret, Prediction and manipulation of hydrodynamic rogue waves via nonlinear spectral engineering, Phys. Rev. Fluids **7**, 054401 (2022).

[60] A. Romero-Ros, G. C. Katsimiga, P. G. Kevrekidis, B. Prinari, G. Biondini, and P. Schmelcher, On-demand generation of dark-bright soliton trains in bose-einstein condensates, Phys. Rev. A **105**, 023325 (2022).

[61] D. Kraus, G. Biondini, and G. Kovačič, The focusing Manakov system with nonzero boundary conditions, Nonlinearity **28**, 3101 (2015).

[62] F. Baronio, A. Degasperis, M. Conforti, and S. Wabnitz, Solutions of the Vector Nonlinear Schrödinger Equations: Evidence for Deterministic Rogue Waves, Phys. Rev. Lett. **109**, 044102 (2012).

[63] A. A. Raskovalov and A. A. Gelash, Resonant interactions of vector breathers, JETP Lett. **115**, 45 (2022).

[64] W.-J. Che, S.-C. Chen, C. Liu, L.-C. Zhao, and N. Akhmediev, Nondegenerate Kuznetsov-Ma solitons of Manakov equations and their physical spectra, Phys. Rev. A **105**, 043526 (2022).

[65] D. S. Agafontsev and V. E. Zakharov, Integrable turbulence and formation of rogue waves, Nonlinearity **28**, 2791 (2015).

[66] M. Conforti, S. Li, G. Biondini, and S. Trillo, Auto-modulation versus breathers in the nonlinear stage of modulational instability, Opt. Lett. **43**, 5291 (2018).

[67] A. E. Kraych, D. Agafontsev, S. Randoux, and P. Suret, Statistical Properties of the Nonlinear Stage of Modulation Instability in Fiber Optics, Phys. Rev. Lett. **123**, 093902 (2019).

[68] A. A. Gelash, D. Agafontsev, V. E. Zakharov, G. El, S. Randoux, and P. Suret, Bound State Soliton Gas Dynamics Underlying the Spontaneous Modulational Instability, Phys. Rev. Lett. **123**, 234102 (2019).

[69] A. M. Perego, F. Bessin, and A. Mussot, Complexity of modulation instability, Phys. Rev. Research **4**, L022057 (2022).

[70] N. N. Akhmediev, L. L. Betina, V. M. Eleonskiĭ, N. E. Kulagin, N. V. Ostrovskaya, and É. A. Poltoratskĭ, Optimal self-compression of multisoliton pulses in an optical fiber, Sov. J. Quantum Electron. **19**, 1240 (1989).

[71] A. V. Slunyaev and E. N. Pelinovsky, Role of Multiple Soliton Interactions in the Generation of Rogue Waves: The Modified Korteweg–de Vries Framework, Phys. Rev. Lett. **117**, 214501 (2016).

[72] A. V. Slunyaev, On the optimal focusing of solitons and breathers in long-wave models, Stud. Appl. Math. **142**, 385 (2019).

[73] C. Liu, Z.-Y. Yang, W.-L. Yang, and N. Akhmediev, Chessboard-like spatio-temporal interference patterns and their excitation, J. Opt. Soc. Am. B **36**, 1294 (2019).